NEAR-SHORE DOPPLER CURRENT METER WAVE SPECTRA[1]

Lee Gordon[2] and Atle Lohrmann[3]

Abstract: We compare PUV wave observations from two collocated velocity/pressure sensors (Aquadopp Current Profiler and Vector Velocimeter). Our objective was to use the differences in the two sensors to evaluate their performance. We evaluate limitations and uncertainties in the wave measurements, focusing particularly on the high frequency cutoff and uncertainties in direction and spreading. We model direction and spreading uncertainties with a simple Monte Carlo simulation, which compares well with our wave data. We conclude that either instrument is able to observe wave spectra and wave height with an uncertainty of a few percent and with wave direction uncertainties of a few degrees.

INTRODUCTION

PUV wave sensors have long been important instruments for observing shallow-water directional wave spectra. New Doppler velocity sensors combined with high resolution pressure sensors are improving our ability to make PUV measurements—they make it easier and less costly and they provide better results.

The following presents results from two such sensors, the Aquadopp Current Profiler and the Vector Velocimeter, both manufactured by Nortek AS. Because they were deployed side-by-side, they observed the same waves, but with different performance and noise characteristics. We use the simultaneous results to explore the Aquadopp's and Vector's measurement uncertainties and limitations. In particular, we model PUV direction and spreading errors with a simple Monte Carlo simulation, and we find that the model reflects well the actual performance of these sensors.

DATA

Deployment and Data Processing

The Aquadopp and Vector were deployed side-by-side in 8 m of water offshore Torrey Pines Beach just north of La Jolla, CA. The Aquadopp and Vector both observe velocity acoustically, but they do so differently. The Aquadopp measures current velocity in multiple levels over roughly a 10 m depth range, while the Vector is designed to measure velocity rapidly and with high precision in a small cell.

---

[1] This document has been revised from a paper published in the ASCE Waves2001 proceedings. Figures have been revised from black and white to color, the original Figure 4 has been replaced by Figures 4a and 4b, and Figure 10b has been added. The additional figures were not included in the original Waves2001 paper because its length is limited to 10 pages.

[2] NortekUSA, 9948 Hibert St., San Diego, CA 92131, 858-586-0900; fax: 858-586-0110; lgordon@nortekusa.com

[3] Nortek AS, Industrieveien33, N-1337 Sandvika, Norway, 47-67-556-200; fax: 47-67-54-61-50; inquiry@nortek.no

The Aquadopp used its wave observation mode to measure velocity in a single 2 m cell centered 2.2 m above the its pressure sensor. The Vector's 14 mm velocity cell was centered about 0.45 m above its pressure sensor (Figure 1). The two instruments were separated horizontally by 0.5 m on an OceanScience Sea Spider frame.

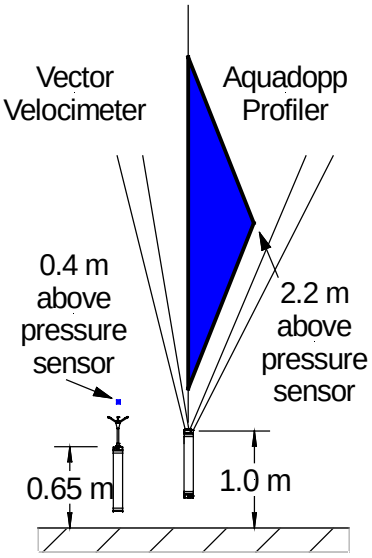

Figure 1. Location of velocity cells for the Aquadopp Profiler (blue triangle) and the Vector Velocimeter (small blue spot). The dimensions at the bottom of the figure give the elevations of the pressure sensors above the sand.

The instruments collected overlapping 2048-point 2-Hz time series every 2 hours over a period of 48 hours. These are the 24 time intervals to which we will refer below.

We use linear wave theory to convert velocity and pressure spectra to surface elevation spectra. We converted pressure (C_{pp}) and velocity (C_{uu}) power spectra to surface elevation power spectra with the following equations:

$$C_{\eta\eta p} = \left[\frac{\cosh kh}{\cosh k(h+z)}\right]^2 \frac{C_{pp}}{\rho^2 g^2} \tag{1}$$

$$C_{\eta\eta u} = \left[\frac{\sinh kh}{\cosh k(h+z)}\right]^2 \frac{C_{uu}}{\sigma^2} \tag{2}$$

where $C_{\eta\eta p}$ and $C_{\eta\eta u}$ are surface elevation (η) spectra based on pressure (p) and velocity (u), k is wavenumber, h is mean water level relative to the seabed, z is the vertical distance relative to the mean water level (positive up), σ is frequency, ρ is water density and g is gravity. Note that the $\rho^2 g^2$ scaling in (1) is already built into the Aquadopp and Vector pressure data, both of which report depth instead of pressure.

Wavenumber and frequency are related according to the usual surface wave dispersion relation:

$$\sigma^2 = gk \tanh kh \tag{3}$$

We compute direction D using

$$D = \text{atan2}\ (C_{pu}, C_{pv}) \tag{4}$$

where atan2 is a 4-quadrant arctangent, and C_{pu} and C_{pv} are the real parts of the pressure-velocity cross-spectra for the u (east) and v (north) velocity components, respectively. Because the pressure and velocity are entirely independent measurements, there is no obvious source of bias in the estimate of direction unless the velocity measurements are themselves biased (i.e. by nearby obstructions). In fact directional measurements similar to (4) have been long known to be robust (Barstow and Krogstad 1984).

We computed wave spreading S using

$$S = \left(\frac{1 - R}{2} \right)^{0.5} \qquad \text{where} \qquad R = \left(\frac{(C_{uu} - C_{vv})^2 + 4C_{uv}^2}{(C_{uu} + C_{vv})^2} \right)^{0.5} \tag{5}$$

Where C_{uu} and C_{vv} are velocity component power spectra and C_{uv} is the cross spectrum of the u and v velocity components (Krogstad et al., 1998). This equation produces results that are similar to the equation used, for example, in Herbers et al. (1999), and it is easier to implement.

Observations

Figure 2 shows typical velocity and pressure time series measured by the Aquadopp and Vector. The similarity in the data is the result of the close proximity of the sensors. The visible difference between the velocity measurements is largely the result of the different size and shape of the velocity cells. In contrast, the two pressure sensors are nearly collocated.

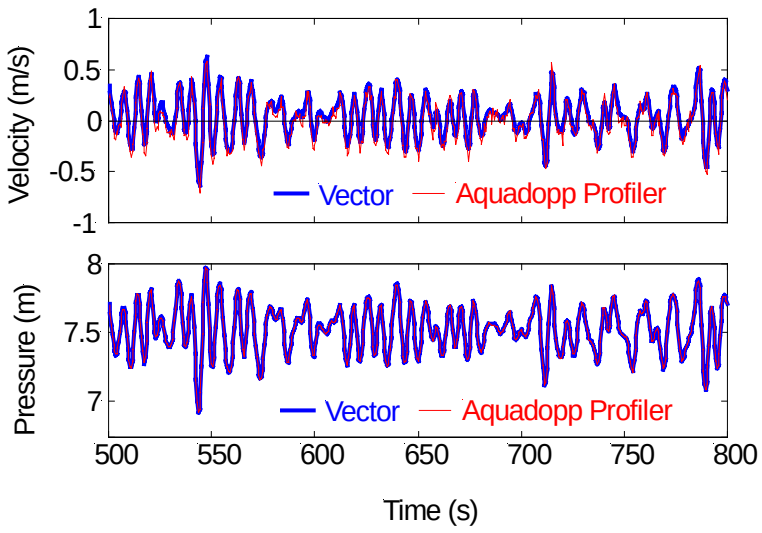

Figure 2. Typical velocity and pressure time series showing 7-s waves measured by the Vector and the Aquadopp. Small differences in these time series are apparent in velocity but harder to see in the pressure, which overlap each other nearly exactly.

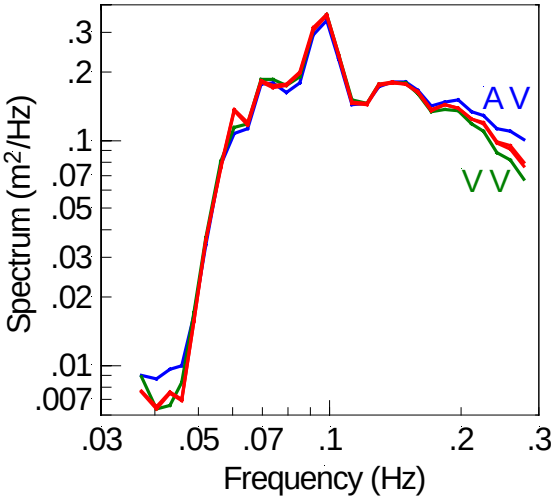

Figure 3. Surface wave spectra computed from velocity and pressure sensors. The pressure spectra are in red and overlap each other almost exactly. The letters "VV" mark the wave spectrum using the Vector Velocity and the letters "AV" mark the spectrum using the Aquadopp Velocity. These spectra are averages of the spectra from all 24 time intervals. The spectra were cut off just below 0.3 Hz (see later).

A) Vector

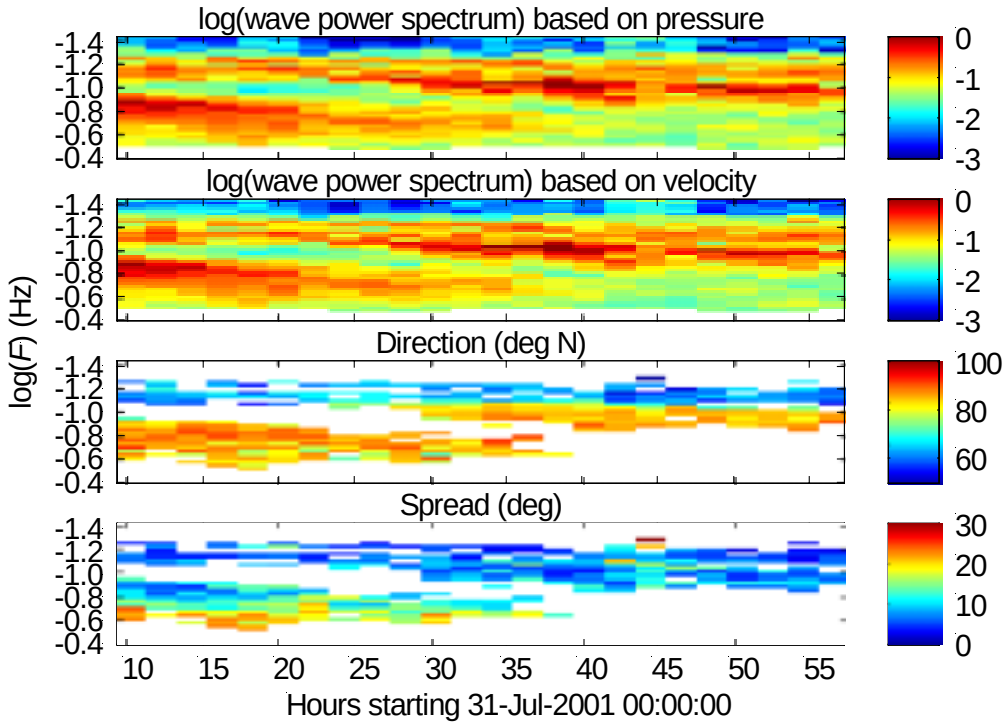

B) Aquadopp

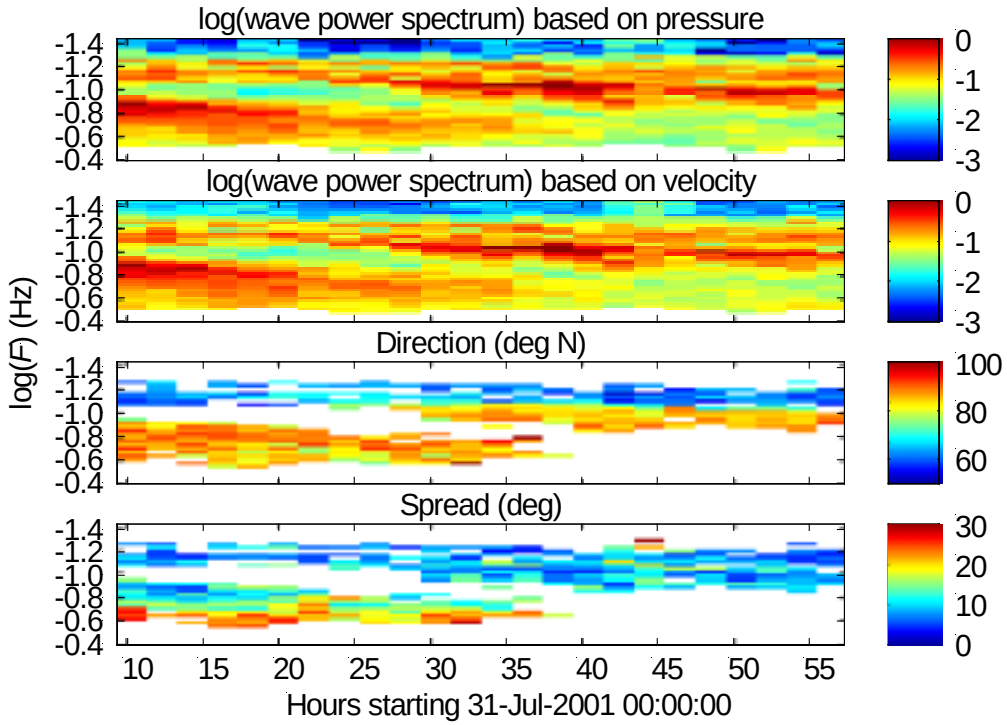

Figure 4. Evolution over all 24 time intervals of the wave spectra, wave direction and wave spreading. Top: Vector; Bottom: Aquadopp. The two data sets were collected simultaneously.

Figure 3 shows that the mean wave spectra, computed using (1) and (2) are nearly identical. The spectra were averaged for this and subsequent displays using "log averaging", for which the averaging bandwidth increases logarithmically with frequency.

The time evolution of the Aquadopp and Vector wave spectra is displayed in Figure 4. The two data sets look virtually identical. There are three discernable "events":

1) Wave periods 5-8 s (log*(F)*=-0.7 to -0.9), heading roughly onshore, and covering most of the first half of the measurement period
2) Wave periods 8-15 s (log*(F)*=-0.9 to -1.2), heading roughly onshore, and covering roughly the latter 2/3 of the measurement period
3) Wave periods 12-18 s (log*(F)*=-1.1 to -1.25), heading to the north of onshore and covering the entire measurement period. This event is easier to discern in a color version of Figure 3.

Figure 5 shows the significant wave height (H_s) and wave parameters at the peak of the spectrum, plus the water level. The significant wave heights observed by the Aquadopp and Vector were the same within a fraction of a percent. The peak periods and directions jump back and forth a little, reflecting a "competition" among the three "events" listed above.

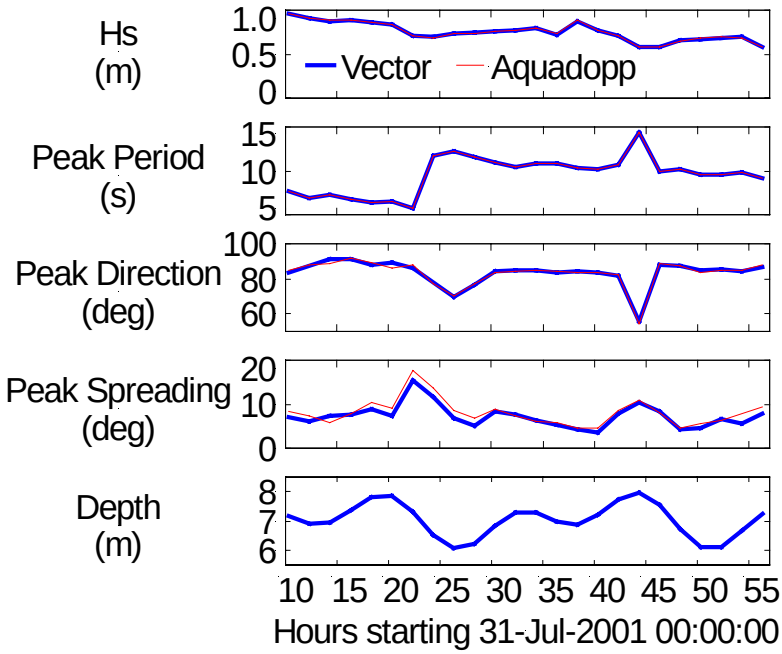

Figure 5. Integral wave parameters computed for each of the 24 time intervals. Significant wave height, Hs, is four times the standard deviation in the wave frequency band 0.035-0.3 Hz. Peak Period, Direction and Spreading are computed at the peak of each spectrum.

Figure 6 compares wave direction and spreading observed by the Aquadopp and the Vector. The directions have been plotted after a mean difference of 3.7° was removed. The mean difference can be attributed to compass uncertainty combined with uncertainty in the mounting of the Vector's cable probe relative to the compass. The standard deviation of the difference between the two instruments' direction measurements was 2.2°. The standard deviation of the difference between the two instruments' wave spreading measurements was 1.7° and the Aquadopp spreading was biased larger by 1.6°.

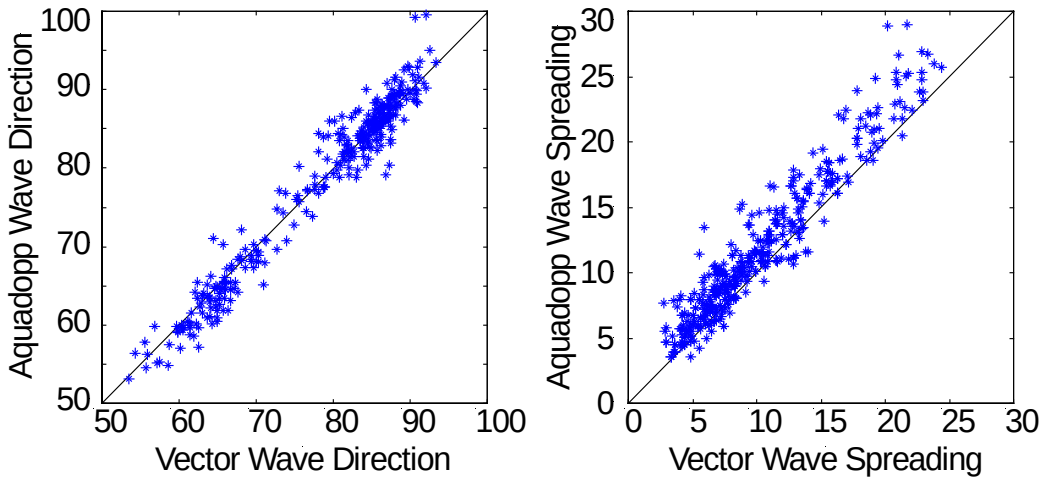

Figure 6. Comparison of Aquadopp and Vector wave direction (left) and wave spreading (right). Data are taken from frequency bands in the spectra from each of the 24 time intervals conditioned on the spectrum being greater than 0.1 m^2/Hz.

UNCERTAINTIES AND LIMITATIONS

The PUV method involves limitations and uncertainties, as do all measurement methods. This section explores the high-frequency cutoff associated with scaling up measurements made deep beneath the surface and presents a model for uncertainties in direction and spreading estimates. The results should apply to any unbiased velocity/pressure sensor—the fact that the Aquadopp and Vector measure velocity differently enable us to evaluate the model.

Wave Spectrum and Significant Wave Height

The magnitude of the wave spectrum is sensitive to the position of the sensors and the overall water depth; it is more sensitive to the uncertainty in the depth of each sensor, and less sensitive to the total water depth. This paper does not explore this sensitivity in detail, but the results suggest that it should be possible to obtain spectra and wave heights with an overall uncertainty of a few percent—the results of our observations agreed to within less than a percent. One may compare velocity and pressure spectra as a sanity check for the installation and overall water depths; one may also compare spectra by varying these depths over the range of uncertainty to quantify the uncertainty of the spectrum and wave height.

High-frequency Cutoff.

This section shows how the original raw spectra are converted, via scaling factors, to wave spectra. The spectra in Figure 6 show that the Aquadopp's velocity has the highest noise floor at 3×10^{-3} m^2/s^2/Hz. The other measurements noise levels fall below the turbulence. None of the measurements fall to their noise floors within the observable wave spectrum, so the noise levels in this case appear not to be significant factors in the wave cutoff. These spectra provide a basis for computing SNR, which is much higher for the pressures and the Vector velocity than for the Aquadopp velocity.

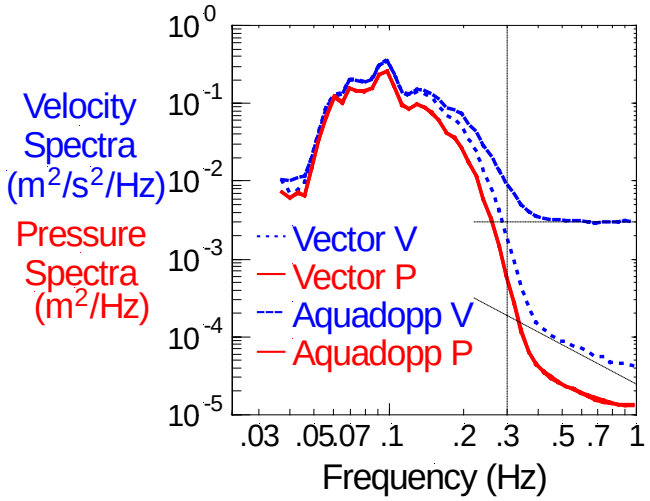

Figure 6. Raw velocity and pressure power spectra show the noise characteristics of the various measurements. The vertical dashed line at 0.3 Hz is the spectral cutoff. The flat dashed line at 3×10^{-3} $m^2/s^2/Hz$ is the noise level of the Aquadopp velocity. The sloping dashed line shows a spectrum with a –5/3 power law, as would be typical of the turbulent inertial subrange.

Figure 7 shows how the scale factors, which convert pressure and velocity to wave spectra, must blow up to compensate for rapidly increasing depth attenuation at high frequencies. The cutoff comes at the inflection point where the increasing scale factor overcomes the falling wave spectrum. The cutoff is sharply defined because the scale factors grow quickly with frequency.

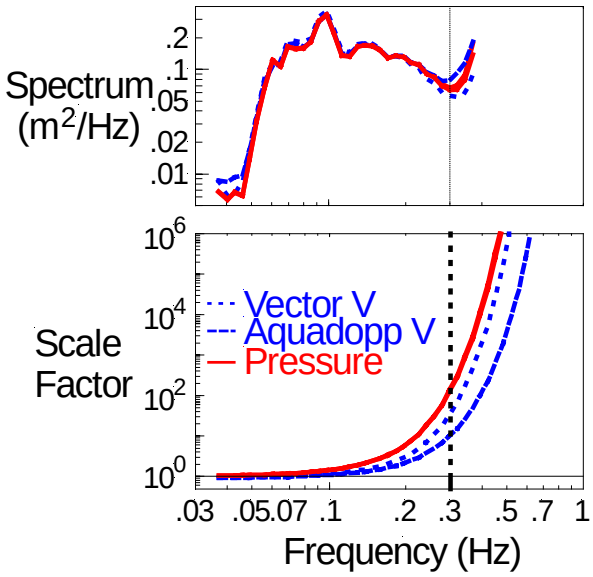

Figure 7. Scaling and spectral cutoff. The bottom panel shows how the velocity and pressure scale factors grow with frequency. The growth in the scale factors corresponds to the increased attenuation that occurs at high frequencies. As these scale factors grow they cause the computed wave spectra to blow up. The cutoff (vertical dashed line) is taken at the inflection point of the spectra where they blow up.

The scale factor units are pressure (dimensionless) and velocity (s^2).

Figure 8 shows how the high-frequency cutoff depends on depth. This curve is obtained by limiting the pressure scale factor to 200 and it does not take into account the sensor's noise levels.

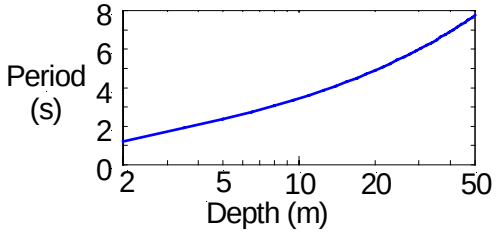

Figure 8. An approximate relationship between the high frequency cutoff and the water depth. Here we assume that the sensor is placed 1 m above the bottom and that the pressure scale factor is allowed to grow to 200.

Direction and Spreading Uncertainty

Direction and spreading uncertainty depends on the directional distribution, the SNR (signal/noise ratio), and the amount of averaging (degrees of freedom, ν). In the following, we assume that waves come from a single direction, and that they are spread narrowly (we investigate spreading up to 30°).

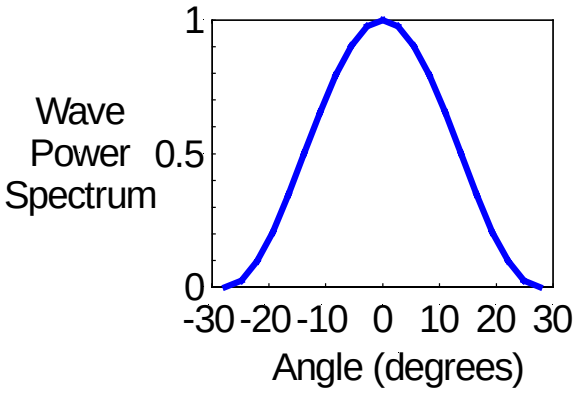

Figure 9. Assumed spreading distribution for a spreading of 10 degrees.

We investigate these uncertainties with a simple Monte-Carlo simulation. We modeled wave spreading using the cosine-squared distribution shown in Figure 9. We constructed synthetic time series by combining 21 random velocity vector time series with directions spaced uniformly over the direction range, and with power spectra that depended on direction as in Figure 9. We simulated varying SNR by adding varying amounts of white noise to the velocity data, equally to both components. We then computed direction and spreading using (5) and (6), creating independent averages with varying ν (using the log averaging as described earlier). We ran a few simple tests to see how sensitive the results were to the nature of the distribution (e.g. substituting a rectangular distribution), and we found that the results did not change much. All-in-all, we ran the simulation with around 25000 independent time series. The results of the simulation are shown in Figures 10a and 10b, for averages with $\nu = 2$. The simulated standard deviations of both direction and spreading fall slightly faster than $\nu^{-0.5}$, but the actual standard deviations almost certainly fall at exactly $\nu^{-0.5}$ (Long 1980). The high-SNR results in The standard deviations in Figure 10a appear to be comparable to Long's results (Krogstad 1991); our simulation includes dependence on SNR, which was not evaluated by Long.

There is no apparent bias in the direction estimate. Figure 10b shows that the spreading estimate is biased low for high SNR: bias is smaller than -1° for spreading less than 10°, but bias increases to -8° for spreading of 30°. Spreading bias begins to increase when SNR falls below around 100, particularly when spreading is small.

The model standard deviations for direction and spreading can be approximated with the following equations:

$$\sigma(D) = \frac{(S + 80/SNR^{0.5})}{\nu^{0.5}} \tag{6}$$

$$\sigma(S) = \min\left(\left[\frac{8S}{\nu} + 10^4\left(2 + SNR^{.25}\right)^{-4}\right]^{.5}, 11°\right) \tag{7}$$

Where σ represents the standard deviation.

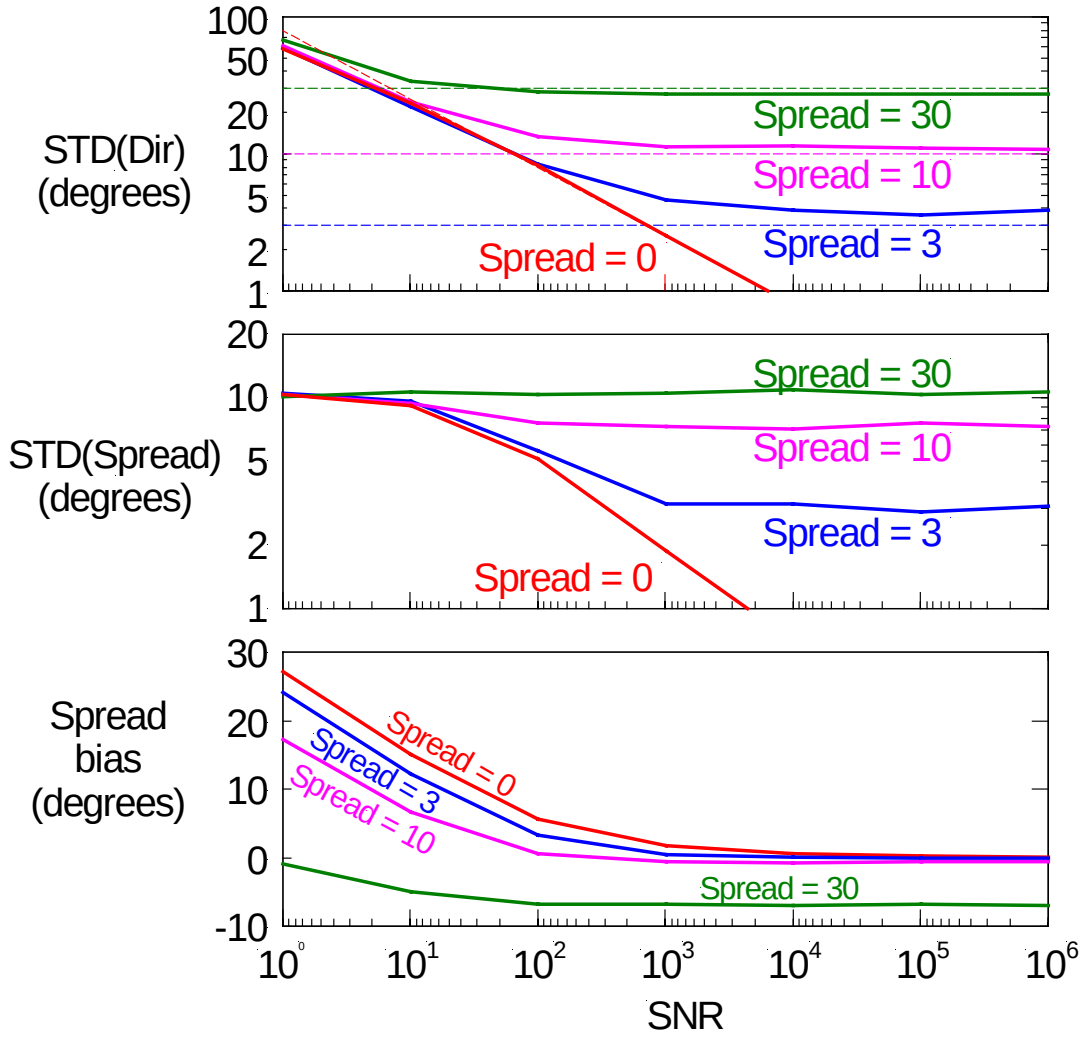

Figure 10a. Direction and spreading uncertainty vs. SNR with four different assumed spreading functions. The plots are based on averages using ν = 2. There was no apparent bias in the direction estimate.

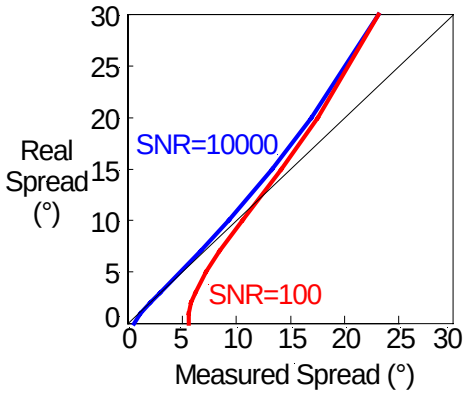

Figure 10b. Detail: spreading bias for high and moderate SNR.

Table 1. Observed wave statistics during three events. *

Event	Inst.	Per. Range	Hours	N	<ν>	SNR	<D>	<S>	σ(D)	σ(S)	Predicted σ(D)	Predicted σ(S)
1		5-7.7 s	9-27	60	19	3600	87.3	12.3	3.0	3.9	2.2	3.3
2	Vector	8.2-10.2 s	29-53	47	12	7500	84.9	8.3	2.2	2.8	2.0	3.4
3		12.6-17.8 s	41-55	32	6	3800	62.3	7.5	3.7	4.4	3.0	4.6
1		5-7.7 s	9-27	60	19	71	87.6	13.6	3.5	4.2	3.6	3.3
2	Aquadopp	8.2-10.2 s	29-53	47	12	123	84.9	9.4	2.7	3.0	3.4	3.4
3		12.6-17.8 s	41-53	32	6	61	61.5	7.5	4.2	4.4	6.0	4.6

** The event numbers correspond to the list near Figure 4. "Period Range" and "Hours" define the time and frequency range for the events, "N" gives the number of direction and spreading estimates obtained during each event, and "ν" gives the average number of Degrees of Freedom in each estimate. SNR is the ratio of the average wave spectrum across the event to the velocity noise level (3×10^{-3} $m^2/s^2/Hz$ for the Aquadopp and 5×10^{-5} $m^2/s^2/Hz$ for the Vector). "<D>" and "<S>" are the averages of the N direction and spreading estimates, respectively. "σ(D)" and "σ(S)" are the corresponding standard deviations.*

Comparison with Data

To test our uncertainty model, we focused on the three events listed near Figure 4. We reduced the extent, in frequency and time, of the events to eliminate overlaps, leaving smaller events during which waves appear to come from one direction, and wave direction and spreading appear stationary. Table 1 defines the boundaries of the three events, lists statistical parameters and results for direction and spreading in each event and lists the corresponding predicted standard deviations.

Figure 11 shows how the statistical results of our observations compare with predictions from our model. Observed and predicted standard deviations are about equal to each other.

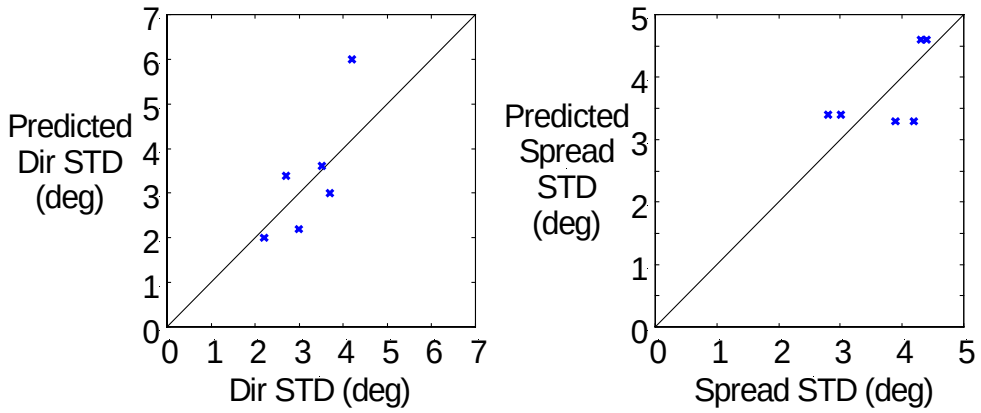

Figure 11. Observed and predicted standard deviations. Observed values come from Table 1 while predicted values are based on (6) and (7).

The results in Table 1 are also consistent with the predicted biases based on our model. The three (Aquadopp-Vector) differences in the mean directions have a standard deviation of about 0.5°, about equal to the value that would be predicted by the model taking into account the number N of direction estimates in each "event". This result is consistent with the lack of bias in the direction measurement and suggests that both instruments are capable, ultimately, of resolving wave direction to less than 1°.

The Aquadopp spreading estimates are about a degree higher on average than the Vector estimates, which is roughly consistent with the different SNRs of the Aquadopp and Vector.

Sources of Direction Bias

The analyses we have done here apply to sensors that are free of biases. The main measurement biases that could turn into a direction bias include differences in the response among the two velocity components, or flow interference from a nearby structure or from the current meter itself. Both the Aquadopp and Vector have the advantage of making measurements remotely. Remote measurements provide many more choices for avoiding these biases. This is one underlying reason for the close agreement in the Aquadopp and Vector wave directions. This leaves the uncertainty of the compass itself (around 2°) as the largest remaining source of bias.

CONCLUSIONS

We explore PUV directional wave spectrum measurement by comparing observations made by two new, high performance Doppler velocity sensors and by comparing the results with a simple Monte Carlo error simulation. We conclude that these instruments are capable of measuring wave spectra and wave height with an uncertainty on the order of a few percent and, with sufficient averaging, capable of measuring wave direction from localized sources with an uncertainty (standard deviation) of less than 1°.

Because our observations and our Monte Carlo model matched each other well, we conclude that the model, particularly Figure 10 and equations 6 and 7, serves well as a means to estimate uncertainties in PUV measurements. In fact the model should apply to any PUV observations so long as the sensor is free of measurement biases.

ACKNOWLEDGEMENTS

We sincerely appreciate the useful comments of Harald Krogstad and Don Resio.

REFERENCES

Barstow, S. F. and H. E. Krogstad 1984. General analysis of directional ocean wave data from heave/pitch/roll buoys. *Mod. Ident. and Control,* 5, 47-70.

Herbers, T. H. C., S. Elgar and R. T. Guza 1999. Directional spreading of waves in the nearshore, *J. Geophys. Res*., 104(4), 7683-7693.

Krogstad, H. E. 1991. Reliability and Resolution of Directional Wave Spectra From Heave, Pitch and Roll Data Buoys, in *Directional Wave Spectra*, Ed. R.C. Beal, Johns Hopkins University Press, 66-71.

Krogstad H. E., S. F. Barstow, O. Haug, and D. J. H. Peters 1998. Directional Distributions in Wave Spectra, *Proc. WAVES'97, Nov. 3-7 1997*, 1, ASCE, 883 - 895.

Long, R. B. 1980. The statistical evaluation of directional estimates derived from pitch/roll buoy data, *J. Phys. Ocean.*, 10, 944-952.

Tucker, M. J. 1989. Interpreting directional data from large pitch-roll-heave-buoys, *Ocean Engineering*, 16, 173-192.